Broken mirror symmetry, incommensurate spin correlations, and B_{2g} nematic order in iron pnictides

Yiming Wang,[1] Wenjun Hu,[2] Rong Yu,[1,*] and Qimiao Si[2,†]

[1]*Department of Physics and Beijing Key Laboratory of Opto-electronic Functional Materials and Micro-nano Devices, Renmin University of China, Beijing 100872, China*

[2]*Department of Physics & Astronomy, Rice Center for Quantum Materials, Rice University, Houston, Texas 77005, USA*

Motivated by recent experiments in the extremely hole doped iron pnictide compounds $A\text{Fe}_2\text{As}_2$ ($A = $ K, Rb, Cs), we consider spin-driven nematic order for incommensurate magnetic fluctuations. We classify the nematic order parameters by broken mirror symmetries of the tetragonal D_{4h} point group, and use this scheme to construct a general Ginzburg-Landau theory that links the nematic order to spatial pattern of magnetic fluctuations. Our analysis points to incommensurate (q, q) magnetic fluctuations as underlying a B_{2g} nematic order in $A\text{Fe}_2\text{As}_2$. We substantiate this idea by microscopic calculations based on three-sublattice $(2\pi/3, 2\pi/3)$ spin correlations in an extended bilinear-biquadratic Heisenberg model. Our classification scheme provides symmetry-based understanding for quasidegeneracy of several nematic channels. The proposed mechanism resolves recently emerged experimental puzzles. We suggest ways to further test it in future experiments and discuss the implications of our results for iron-based high temperature superconductivity.

Introduction. Strongly correlated systems often involve multiple building blocks for their macroscopic properties. Iron-based superconductors (FeSCs) [1–6] provide a prototype example. Typically, the phase diagram contains an antiferromagnetic (AFM) order, pointing to the role of spins. It prominently features a nematic order, which may be driven by spin or other degrees of freedom. Understanding its origin and the associated fluctuations will likely shed light on the mechanism of high temperature superconductivity.

In the most common iron pnictides, an electronic nematic order [7,8] accompanies AF order of wave vector $(\pi, 0)$ [Fig. 1(a)]. It lowers the C_4 rotational symmetry of the tetragonal lattice to C_2 by making the tetragonal a and b axes inequivalent. According to the tetragonal lattice notation, the nematic order has a B_{1g} symmetry. However, nematic order in the FeSCs has considerable variations. The bulk FeSe, for example, has a B_{1g} nematic order which is not accompanied by any AF order [9]. A great deal of effort has recently been devoted to study this nematic order of FeSe.

A new surprise has emerged from heavily hole doped $(\text{Rb,Cs})\text{Fe}_2\text{As}_2$ [10–12]. Recent scanning tunneling microscopy (STM) measurements observe a twofold symmetric quasiparticle interference (QPI) pattern about the two diagonal directions of Fe lattice [10]. Elastoresistance data also reveal an anisotropy along this direction [11]. Both experiments evidence that the nematic order here has a B_{2g} symmetry, which corresponds to a pattern that is rotated from its B_{1g} counterpart by 45°. Equally important, for a range of doping and temperature in $\text{Rb}_x\text{Ba}_{1-x}\text{Fe}_2\text{As}_2$ (x near 0.8), the B_{2g} and B_{1g} nematic channels are nearly degenerate [11].

An important question is whether a universal origin exists for the variety of nematic orders. One candidate mechanism attributes the B_{1g} nematicity to an Ising order that is constructed from AFM or antiferroquadrupolar (AFQ) fluctuations [13–16] at wave vector $(\pi, 0)$ or $(0, \pi)$. To consider the possibility of the B_{2g} nematicity in this light, we are motivated to explore more general types of magnetic fluctuations. Indeed, the spin excitations of KFe_2As_2 [Fig. 1(c)] are peaked near wave vector $(q, 0)$ with $q \approx 2\pi/3$ at low energies, and with increasing energy the wave vector saturates near (q, q). Compared to BaFe_2As_2 [17] and $\text{K}_{0.5}\text{Ba}_{0.5}\text{Fe}_2\text{As}_2$ (see Fig. S2 of the Supplemental Material (SM) [18]), the (q, q) spin excitations occupy a large spectral weight in KFe_2As_2. In addition, $A\text{Fe}_2\text{As}_2$ has been evidenced to move towards an AFM quantum critical point as one goes from $A = $ K to $A = $ (Rb, Cs) [24], making it likely that the (q, q) spin excitations further soften and grow in spectral weight for the (Rb,Cs) cases.

In this Rapid Communication, we are thus motivated to study the role of incommensurate magnetic fluctuations on the nematicity. To this end, we consider the electrons residing on the tetragonal lattice and classify the nematic orders in terms of a broken mirror symmetry to B_{1g}, B_{2g}, and A_{2g}. Building on this symmetry analysis, we propose a general Ginzburg-Landau theory and connect the various nematic orders with the underlying incommensurate magnetic fluctuations. This allows for a unified understanding for the nematicity in FeSCs. In particular, we demonstrate that incommensurate (q, q) and $(-q, q)$ magnetic fluctuations lead to a B_{2g} Ising nematic order. This result is further supported by calculations on a microscopic bilinear-biquadratic Heisenberg model, which find a B_{2g} nematic order from three-sublattice $(2\pi/3, 2\pi/3)$ AFM correlations [Fig. 1(b)]. Finally, through the formulation of broken mirror symmetry, we advance a robust mechanism for a quasidegeneracy between several nematic channels.
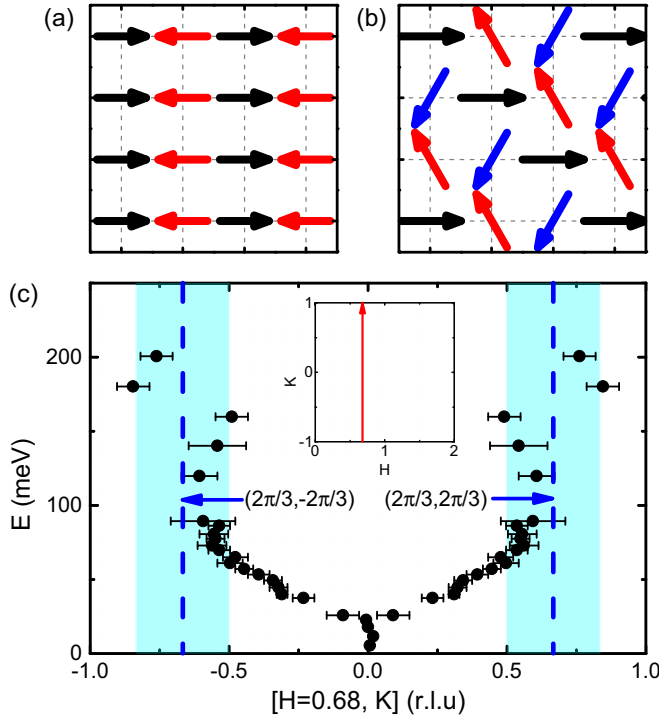
*rong.yu@ruc.edu.cn

†qmsi@rice.edu

FIG. 1. (a),(b) Real space spin patterns of the $(\pi, 0)$ and $(2\pi/3, 2\pi/3)$ AFM states, respectively associated with B_{1g} and B_{2g} nematicity. (c) Dispersion of spin excitations for KFe$_2$As$_2$ measured by inelastic neutron scattering (reproduced from Ref. [22]). The red arrow of the inset specifies the measured cut.

Classification of nematicity. The nematic order of interest breaks a Z_2 symmetry, and is characterized by an Ising variable or a scalar order parameter. It can be classified according to the one-dimensional (1D) irreducible representations of the tetragonal point group (D_{4h}). Since inversion symmetry is preserved, a nematic order should transform as B_{1g}, B_{2g}, or A_{2g}. Each of them is uniquely determined by examining its transformation under the mirror symmetries $\sigma_{x/y}$ and $\sigma_{d/d'}$ [see Table I and Figs. 2(a)–2(c)]. The usual B_{1g} nematic order breaks the mirror plane passing through the diagonal directions ($\sigma_{d/d'}$), but preserves the one through axes ($\sigma_{x/y}$). For the B_{2g} nematic order, the roles of the two mirror planes are reversed. Finally, the A_{2g} nematic order breaks both mirror symmetries $\sigma_{x/y}$ and $\sigma_{d/d'}$ but preserves their product, which is the C_4 symmetry; it qualifies as a nematic state because discrete symmetries such as the C_2 symmetry about either the x or y axis are broken.

Construction of the Ginzburg-Landau theory. We are led to a Ginzburg-Landau theory for the nematicity. Consider

TABLE I. Symmetry classification of nematicity in FeSCs based on the broken mirror symmetries of the D_{4h} group.

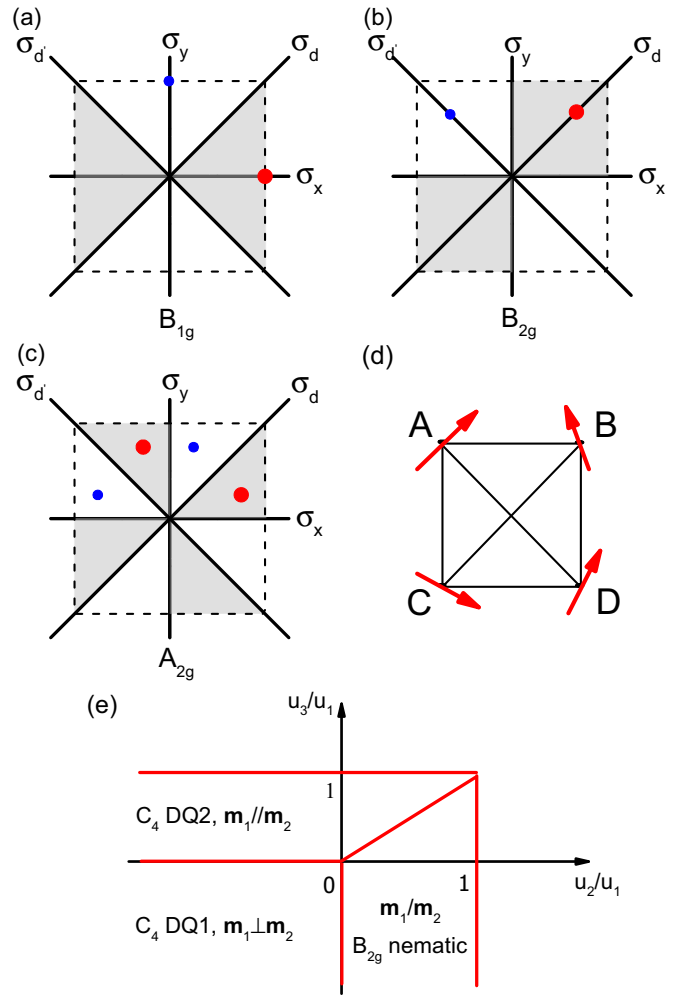| Nematicity	$\sigma_{x/y}$	$\sigma_{d/d'}$	$C_4 = \sigma_{x/y} \times \sigma_{d/d'}$
B_{1g}	1	−1	−1
B_{2g}	−1	1	−1
A_{2g}	−1	−1	1

FIG. 2. (a) Sketch of the B_{1g} function in the 1-Fe Brillouin zone (BZ). The function is positive (negative) in the shaded (white) regime. The dashed frame is the BZ boundary. The solid lines refer to mirror planes through the k_x and k_y directions (σ_x and σ_y) and the diagonal directions (σ_d and $\sigma_{d'}$). The red and blue dots show the magnetic moments associated with the B_{1g} nematicity. (b),(c) Similar sketches for B_{2g} and A_{2g} symmetries, respectively. (d) Illustration of a plaquette in real space with spins. (e) Ground-state phase diagram of the Ginzburg-Landau free energy for B_{2g} nematicity in Eq. (4). The red solid lines show the phase boundaries. $\mathbf{m}_1/\mathbf{m}_2$ refers to a single-Q phase with B_{2g} nematicity, with either $\mathbf{m}_1$ or $\mathbf{m}_2$ being ordered; DQ1 (DQ2) refers to a double-Q phase with C_4 symmetry where $\mathbf{m}_1 \perp \mathbf{m}_2$ ($\mathbf{m}_1 \parallel \mathbf{m}_2$).

an incommensurate magnetic moment $\mathbf{m}_1 = \mathbf{m}(q_1, q_2)$ with a generic wave vector (q_1, q_2) and the other three moments related by mirror symmetries, $\mathbf{m}_2 = \mathbf{m}(-q_2, q_1)$, $\mathbf{m}_3 = \mathbf{m}(q_2, q_1)$, and $\mathbf{m}_4 = \mathbf{m}(-q_1, q_2)$. The Ising-nematic parameters are conventionally defined within each plaquette in real space to be [see Fig. 2(d)] $\sigma_{B1} = (\mathbf{S}_A - \mathbf{S}_D) \cdot (\mathbf{S}_B - \mathbf{S}_C)$ and $\sigma_{B2} = \mathbf{S}_A \cdot \mathbf{S}_D - \mathbf{S}_B \cdot \mathbf{S}_C$. In momentum space, we can write

$$\sigma_{B1} \sim \mathbf{m}_1^2 + \mathbf{m}_4^2 - \mathbf{m}_2^2 - \mathbf{m}_3^2, \tag{1}$$

$$\sigma_{B2} \sim \mathbf{m}_1^2 + \mathbf{m}_3^2 - \mathbf{m}_2^2 - \mathbf{m}_4^2, \tag{2}$$

$$\sigma_{A2} \sim \mathbf{m}_1^2 + \mathbf{m}_2^2 - \mathbf{m}_3^2 - \mathbf{m}_4^2. \tag{3}$$

Since it preserves $\sigma_{d/d'}$, the B_{2g} nematic order is naturally connected to magnetic moments $\mathbf{m}_1 = \mathbf{m}(q, q)$ and $\mathbf{m}_2 = \mathbf{m}(-q, q)$ that have the same symmetry [Fig. 2(b)]. We can then construct an effective Landau free energy as follows:

$$f_{B2} = \frac{r_{B2}}{2}\left(\mathbf{m}_1^2 + \mathbf{m}_2^2\right) + \frac{u_1}{4}\left(\mathbf{m}_1^2 + \mathbf{m}_2^2\right)^2$$
$$- \frac{u_2}{2}\left(\mathbf{m}_1^2 - \mathbf{m}_2^2\right)^2 - \frac{u_3}{2}(\mathbf{m}_1 \cdot \mathbf{m}_2)^2. \quad (4)$$

This construction parallels that for B_{1g} nematicity [21]. The ground state phase diagram [Fig. 2(e)] has an incommensurate AFM order at either (q, q) or $(-q, q)$ when $u_2 > 0$ and $u_2 > u_3$. Since $\mathbf{m}_1^2 - \mathbf{m}_2^2 \propto \sigma_{B2}$, this phase supports a B_{2g} nematic order at finite temperature. There are two additional incommensurate double-Q phases, with $\mathbf{m}_1 \parallel \mathbf{m}_2$ and $\mathbf{m}_1 \perp \mathbf{m}_2$, respectively. They are analogies of the two double-Q AFM phases in the B_{1g} case [21,25], and are expected to have enhanced B_{2g} nematic susceptibility.

We can construct a general free energy for both the B_{1g} and B_{2g} nematicity in terms of the relevant $(q, 0)/(0, q)$ and $(q, q)/(-q, q)$ magnetic moments:

$$f = f_{B1} + f_{B2} + f_{12}, \quad (5)$$

$$f_{B1} = \frac{r_{B1}}{2}\left(\mathbf{m}_3^2 + \mathbf{m}_4^2\right) + \frac{v_1}{4}\left(\mathbf{m}_3^2 + \mathbf{m}_4^2\right)^2$$
$$- \frac{v_2}{2}\left(\mathbf{m}_3^2 - \mathbf{m}_4^2\right)^2 - \frac{v_3}{2}(\mathbf{m}_3 \cdot \mathbf{m}_4)^2, \quad (6)$$

$$f_{12} = w_1\left(\mathbf{m}_1^2 + \mathbf{m}_2^2\right)\left(\mathbf{m}_3^2 + \mathbf{m}_4^2\right) + w_2[(\mathbf{m}_1 \cdot \mathbf{m}_3)^2$$
$$+ (\mathbf{m}_2 \cdot \mathbf{m}_3)^2 + (\mathbf{m}_1 \cdot \mathbf{m}_4)^2 + (\mathbf{m}_2 \cdot \mathbf{m}_4)^2], \quad (7)$$

where $\mathbf{m}_3 = \mathbf{m}(q, 0)$ and $\mathbf{m}_4 = \mathbf{m}(0, q)$. The phase diagram is even richer (see SM [18]), containing single-Q AFM states with either $\mathbf{m}_i$ being ordered, which supports either B_{1g} or B_{2g} nematic order, and several double-Q AFM states with C_4 symmetry. The states with ordered moments $\mathbf{m}_{1/2}$ and $\mathbf{m}_{3/4}$ either are separated by a bicritical point or coexist, depending on the model parameters (see SM [18]).

Bilinear-biquadratic Heisenberg model. We now turn to a microscopic model. A bilinear-biquadratic Heisenberg model has successfully explained the B_{1g} nematicity in iron pnictides and iron selenide [16]. Here we reexamine this model and explore the phase diagram. The Hamiltonian reads as

$$H = \sum_{\langle i,j \rangle, \delta} J_\delta \mathbf{S}_i \cdot \mathbf{S}_j + K_\delta (\mathbf{S}_i \cdot \mathbf{S}_j)^2, \quad (8)$$

where $\delta = 1, 2, 3$, and the summation is up to the third-nearest neighbors. We set $J_1 = 1$ as the energy unit. The frustrating interactions cause a rich phase diagram even in the classical spin limit (see SM). Figure 3(a) shows the ground-state phase diagram for $J_3 = 0.1$, $K_2 = K_3 = 0$, and varying J_2 and K_1. A $(\pi, 0)/(0, \pi)$ AFM occurs when $J_2 > J_1/2$ and $K_1 < 0$. A double-Q C_4 AFM state with $\mathbf{m}(\pi, 0) \perp \mathbf{m}(0, \pi)$ is stabilized when $K_1 > 0$. We find that increasing K_1 while decreasing J_2 stabilizes a (π, q) and further a (q, q) AFM state. Here, the (q, q) AFM state is stabilized due to the competition of J_1 and K_1, which is different from what happens in the classical $J_1 - J_2 - J_3$ model [26]. The incommensurate (q, q) state does support a B_{2g} nematic order below a transition temperature as shown in the Monte Carlo result in Fig. 3(b).
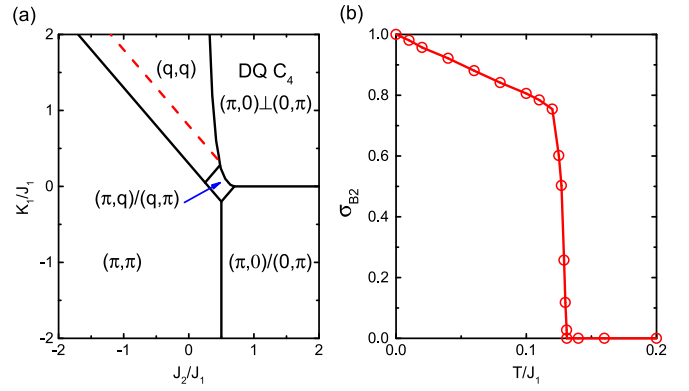
FIG. 3. (a) Ground-state phase diagram of the classical bilinear-biquadratic model for $J_3/J_1 = 0.1$ and $K_2 = K_3 = 0$. The solid black curves show the phase boundaries. Along the dashed red line, the ground state is a $(2\pi/3, 2\pi/3)$ AFM state. (b) Temperature dependence of the B_{2g} nematic order at $J_2 = 0$ and $K_1/J_1 = 0.8$, where the ground state is the $(2\pi/3, 2\pi/3)$ AFM state.

DMRG study on the quantum $S = 1$ model. We have in addition investigated the $S = 1$ bilinear-biquadratic Heisenberg model, Eq. (8), by the density matrix renormalization group (DMRG) method. Including quantum fluctuations makes the phase diagram even richer, with several magnetic and quadrupolar phases, as well as a nematic spin liquid [27]. We find evidence for a robust three-sublattice $(2\pi/3, 2\pi/3)$ AFM phase, signaled by a clear peak at momentum $(2\pi/3, 2\pi/3)$ of the spin structure factor (Fig. 4, inset). This phase can be stabilized for $J_2 = J_3 = K_2 = 0$, $K_1 = 0.8$, and $-0.4 \lesssim K_3 \lesssim -0.1$, a parameter regime close to that in the classical model. This phase supports a B_{2g} nematic order. As shown in Fig. 4, main panel, the B_{2g} nematic order, σ_{B2}, scales to a nonzero value in the thermodynamic limit.

Degeneracy of nematic channels. The advantage of the mirror symmetry formulation is even clearer for the generic $q_1 \neq q_2$ case. There are four moments, $\mathbf{m}_1 = \mathbf{m}(q_1, q_2)$ and
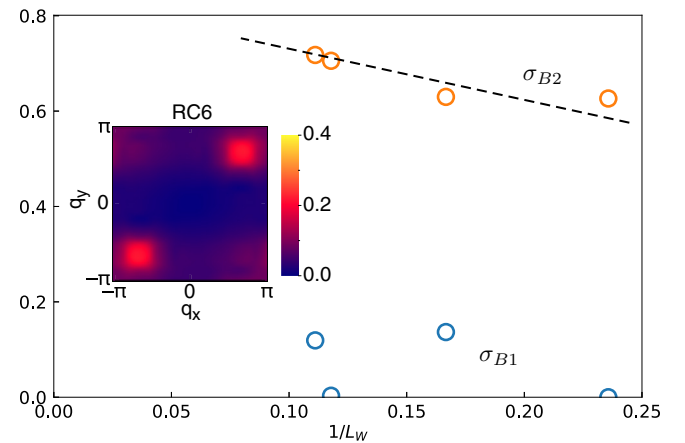
FIG. 4. Finite-size scaling of the nematic order parameters in B_{1g} (orange circles) and B_{2g} (blue circles) channels for the three-sublattice $(2\pi/3, 2\pi/3)$ AFM ground state from DMRG calculation with model parameters $K_1/J_1 = 0.8$, $K_3/J_1 = -0.18$, and $J_2 = J_3 = K_2 = 0$. The dashed line is the guide to the eye. Inset: the spin structure factor of the $(2\pi/3, 2\pi/3)$ AFM ground state on RC6 lattice, which is obtained from the middle of 6×24 sites.

its mirror-symmetry related $\mathbf{m}_2$, $\mathbf{m}_3$, $\mathbf{m}_4$, defined earlier. The Ginzburg-Landau action with D_{4h} symmetry reads

$$S = \sum_{\mathbf{k}} (r + c\mathbf{k}^2) \sum_{i=1,2,3,4} \mathbf{m}_i(\mathbf{k})^2$$

$$+ \int d^2x \left\{ u_1 \sum_i |\mathbf{m}_i|^4 + 2u_2 \sum_{i<j} |\mathbf{m}_i|^2 |\mathbf{m}_j|^2 \right\}, \quad (9)$$

where $\mathbf{m}_i(\mathbf{k}) = \mathbf{m}(\mathbf{q}_i + \mathbf{k})$ with $\mathbf{q}_i = (\pm q_1, \pm q_2)$. A Hubbard-Stratonovich transformation (see SM [18]) yields

$$f \sim r_\sigma \left(\sigma_{B1}^2 + \sigma_{B2}^2 + \sigma_{A2}^2 \right) + b_\sigma \sigma_{B1} \sigma_{B2} \sigma_{A2} + O(\sigma^4). \quad (10)$$

Here, r_σ comes from contributions of magnetic fluctuations and is dictated by symmetry to be identical in each nematic channel. When $r_\sigma > 0$, the nematic fluctuations are exactly degenerate among the three channels, and when $r_\sigma < 0$ a nematic order arises as shown in a large-N calculation in SM [18]. In the nematic phase, either the degeneracy is lifted by spontaneous ordering to one nematic channel or the ordering takes place in all three channels with $\sigma_{B1} = \sigma_{B2} = \sigma_{A2}$. The latter case is due to the cubic term of σ_i in Eq. (10), which reflects the discrete D_{4h} symmetry. Note that the nature of the nematic transition is very different from the magnetic ordering in a Heisenberg or an XY model, where the spontaneous symmetry breaking can take place along any direction in the spin space.

Recent elastoresistance measurement indeed reveals a quasidegeneracy between the B_{1g} and B_{2g} nematic fluctuations in the intermediate hole doping regime of iron pnictides [11]. Neutron scattering measurements [22] show that, upon hole doping, enhanced incommensurate (q_1, q_2) fluctuations appear in the low-energy spin excitation spectrum. Thus this quasidegeneracy is well understood in our theory.

When the (q_1, q_2) type magnetic fluctuations couple to $(q, 0)$ or (q, q) fluctuations, the degeneracy among the three nematic channels can be lifted to a degree. In real materials, magnetic fluctuations couple to other degrees of freedom, such as orbital and lattice, which may also help break the exact degeneracy of the three nematic channels to stabilize a particular type of nematic order [28,29]. Nonetheless, our formulations reveal that the spin-driven nematicity naturally accounts for the observed quasidegeneracy between the B_{1g} and B_{2g} fluctuations. It would also be interesting to explore the possibility of an A_{2g} nematicity in FeSCs.

Discussions and conclusions. We now note on several points. First, the proposed mechanism for a B_{2g} nematicity well accounts for the observations by recent STM, elastoresistance, and NMR measurements in heavily hole doped iron pnictides [10–12]. In our analysis the B_{2g} nematic order is associated with the (q, q)-type incommensurate magnetic fluctuations, which are a large part of the spin spectral weight in KFe$_2$As$_2$ [22]. The three-sublattice $(2\pi/3, 2\pi/3)$ AFM spin order is consistent with that part of the fluctuation spectrum [Fig. 1(c)]. Thermodynamic measurements have suggested that (Rb,Cs) replacement for K drives the system toward an AFM quantum critical point [24]. It is thus likely that the (q, q) AFM fluctuations will be enhanced in the (Rb,Cs) cases, thereby strengthening the B_{2g} correlations. Inelastic neutron scattering measurements in (Rb,Cs)Fe$_2$As$_2$
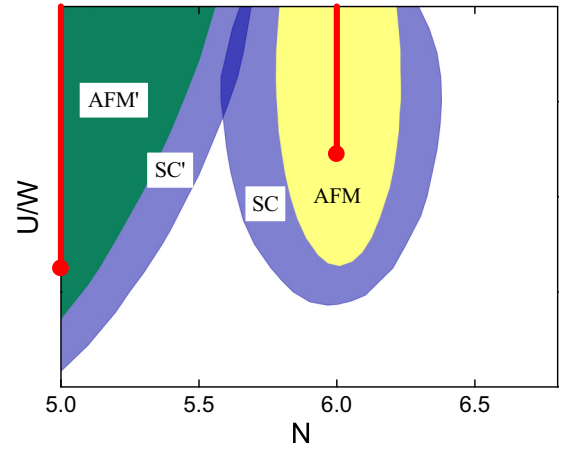

FIG. 5. Schematic phase diagram as a function of the U/W (the ratio of the Coulomb interaction to bandwidth). Here AFM marks the $(\pi, 0)$ AFM order; AFM$'$ represents the (q, q) AFM order, with q reaching π as the electron number per Fe ion $N \to 5$; SC and SC$'$ denote superconductivity. Adapted from Refs. [24,34].

are called for. We note in passing that the phase diagram of the bilinear-biquadratic model also contains a three-sublattice $(2\pi/3, 2\pi/3)$ AFQ order and a double-stripe $(\pi/2, \pi/2)$ AFM order, either of which may support the B_{2g} nematicity [16,30–33].

Second, the softening of (q, q) magnetic fluctuations with hole doping suggests reduced J_2 value from BaFe$_2$As$_2$, which drives the system from the $(\pi, 0)$ to (q, q) AFM order, as shown in Fig. 3(a). The strong electron correlations in (K,Rb,Cs)Fe$_2$As$_2$ make *ab initio* estimates of J's and K's difficult. Still, the (q, q) AFM order is relevant for (K,Rb,Cs)Fe$_2$As$_2$, which has $N = 5.5$ and corresponds to the strongly hole-doped counterpart of the $N = 6$ BaFe$_2$As$_2$. The schematic zero-temperature phase diagram (Fig. 5) [24,34] illustrates that two types of antiferromagnetic orders are respectively associated with the $N = 6$ and $N = 5$–5.5 regimes. Given that the half-filled $N = 5$ case is expected to have a commensurate (π, π) AFM order, it is natural for the $N = 5.5$ to develop the (q, q) AFM order. In this sense, the (q, q) AFM order implicated by our work elucidates the microscopic physics of the FeSCs over an extended doping range.

Third, upon doping alkaline ions, experiments suggest that the low-temperature electronic states may evolve from a B_{1g} nematic state to a double-Q C_4 state [35–37], and to a B_{2g} nematic state. All these states appear in the phase diagrams of our Landau theory as well as in the proposed microscopic model with frustrated bilinear-biquadratic interactions. Thus the proposed mechanism represents a unified description of this rich variety of nematic orders. Because this unified description involves the magnetic degrees of freedom, this overall understanding suggests the important role of spin interactions in promoting the emergent properties of the iron-based materials including their high temperature superconductivity.

Finally, classifying nematic order through broken rotational symmetry goes back to its liquid crystal root. Ours is the first to frame it via broken mirror symmetry, which is natural in crystalline settings. Our approach will likely be important

in the context of electronic topology as well, where nonlocal symmetries such as mirror symmetry play an important role.

In conclusion, we have introduced a framework for nematic orders by broken mirror symmetries. Using this approach, we have advanced a mechanism for a B_{2g} nematic order and for a robust understanding of quasidegenerate nematic channels. The mechanism provides a unified description of nematicity in iron-based superconductors and elucidates the physics of the FeSCs in the heavily hole-doped regime.

[1] Y. Kamihara, T. Watanabe, M. Hirano, and H. Hosono, J. Am. Chem. Soc. **130**, 3296 (2008).

[2] D. C. Johnston, Adv. Phys. **59**, 803 (2010).

[3] P. Dai, Rev. Mod. Phys. **87**, 855 (2015).

[4] Q. Si, R. Yu, and E. Abrahams, Nat. Rev. Mater. **1**, 16017 (2016).

[5] P. J. Hirschfeld, C. R. Phys. **17**, 197 (2016).

[6] F. Wang and D.-H. Lee, Science **332**, 200 (2011).

[7] M. Yi, D. Lu, J.-H. Chu, J. G. Analytis, A. P. Sorini, A. F. Kemper, B. Moritz, S.-K. Mo, R. G. Moore, M. Hashimoto *et al.*, Proc. Natl. Acad. Sci. USA **108**, 6878 (2011).

[8] J.-H. Chu, H.-H. Kuo, J. G. Analytis, and I. R. Fisher, Science **337**, 710 (2012).

[9] Q. Wang, Y. Shen, B. Pan, Y. Hao, M. Ma, F. Zhou, P. Steffens, K. Schmalzl, T. R. Forrest, M. Abdel-Hafiez *et al.*, Nat. Mater. **15**, 159 (2016).

[10] X. Liu, R. Tao, M. Ren, W. Chen, Q. Yao, T. Wolf, Y. Yan, T. Zhang, and D. Feng, Nat. Commun. **10**, 1039 (2019).

[11] K. Ishida, M. Tsujii, S. Hosoi, Y. Mizukami, S. Ishida, A. Iyo, H. Eisaki, T. Wolf, K. Grube, H. v. Löhneysen, R. M. Fernandes, and T. Shibauchi, arXiv:1812.05267.

[12] J. Li, D. Zhao, Y. P. Wu, S. J. Li, D. W. Song, L. X. Zheng, N. Z. Wang, X. G. Luo, Z. Sun, T. Wu, and X. H. Chen, arXiv:1611.04694.

[13] J. Dai, Q. Si, J.-X. Zhu, and E. Abrahams, Proc. Natl. Acad. Sci. USA **106**, 4118 (2009).

[14] C. Fang, H. Yao, W. F. Tsai, J. P. Hu, and S. A. Kivelson, Phys. Rev. B **77**, 224509 (2008).

[15] C. Xu, M. Müller, and S. Sachdev, Phys. Rev. B **78**, 020501(R) (2008).

[16] R. Yu and Q. Si, Phys. Rev. Lett. **115**, 116401 (2015).

[17] L. W. Harriger, H. Q. Luo, M. S. Liu, C. Frost, J. P. Hu, M. R. Norman, and P. Dai, Phys. Rev. B **84**, 054544 (2011).

[18] See Supplemental Material at http://link.aps.org/supplemental/10.1103/PhysRevB.100.100502 for details on the Ginzburg-Landau theory for nematic orders with incommensurate magnetic fluctuations and the evolution of spin excitations with hole doping in $K_xBa_{1-x}Fe_2As_2$, which include Refs. [19–23].

[19] P. M. Chaikin and T. C. Lubensky, *Principles of Condensed Matter Physics* (Cambridge University Press, Cambridge, UK, 1995), Chap. 4.

[20] J. Wu, Q. Si, and E. Abrahams, Phys. Rev. B **93**, 104515 (2016).

[21] R. Yu, M. Yi, B. A. Frandsen, R. J. Birgeneau, and Q. Si, arXiv:1706.07087.

[22] K. Horigane, K. Kihou, K. Fujita, R. Kajimoto, K. Ikeuchi, S. Ji, J. Akimitsu, and C. H. Lee, Sci. Rep. **6**, 33303 (2016).

[23] J. Luttinger and L. Tisza, Phys. Rev. **70**, 954 (1946).

[24] F. Eilers, K. Grube, D. A. Zocco, T. Wolf, M. Merz, P. Schweiss, R. Heid, R. Eder, R. Yu, J.-X. Zhu *et al.*, Phys. Rev. Lett. **116**, 237003 (2016).

[25] G. Giovannetti, C. Ortix, M. Marsman, M. Capone, J. van den Brink, and J. Lorenzana, Nat. Commun. **2**, 398 (2011).

[26] A. Moreo, E. Dagotto, T. Jolicoeur, and J. Riera, Phys. Rev. B **42**, 6283 (1990).

[27] W.-J. Hu, S.-S. Gong, H.-H. Lai, H. Hu, Q. Si, and A. H. Nevidomskyy, arXiv:1711.06523.

[28] C. B. Bishop, A. Moreo, and E. Dagotto, Phys. Rev. Lett. **117**, 117201 (2016).

[29] S. Onari and H. Kontani, Phys. Rev. B **100**, 020507(R) (2019).

[30] C. B. Bishop, J. Herbrych, E. Dagotto, and A. Moreo, Phys. Rev. B **96**, 035144 (2017).

[31] T. A. Tóth, A. M. Läuchli, F. Mila, and K. Penc, Phys. Rev. B **85**, 140403(R) (2012).

[32] H.-H. Lai, S.-S. Gong, W.-J. Hu, and Q. Si, arXiv:1608.08206.

[33] G. Zhang, J. K. Glasbrenner, R. Flint, I. I. Mazin, and R. M. Fernandes, Phys. Rev. B **95**, 174402 (2017).

[34] R. Yu, J.-X. Zhu, and Q. Si, Curr. Opin. Solid State Mater. Sci. **17**, 65 (2013).

[35] J. M. Allred, K. M. Taddei, D. E. Bugaris, M. J. Krogstad, S. H. Lapidus, D. Y. Chung, H. Claus, M. G. Kanatzidis, D. E. Brown, J. Kang *et al.*, Nat. Phys. **12**, 493 (2016).

[36] A. E. Böhmer, F. Hardy, L. Wang, T. Wolf, P. Schweiss, and C. Meingast, Nat. Commun. **6**, 7911 (2015).

[37] S. Avci, O. Chmaissem, J. M. Allred, S. Rosenkranz, I. Eremin, A. V. Chubukov, D. E. Bugaris, D. Y. Chung, M. G. Kanatzidis, J.-P. Castellan *et al.*, Nat. Commun. **5**, 3845 (2014).